Available online at www.sciencedirect.com
SCIENCE DIRECT®
Acta Materialia 53 (2005) 4881–4892
Acta MATERIALIA
www.actamat-journals.com

Mechanical properties of an ultrafine grained C–Mn steel processed by warm deformation and annealing

R. Song, D. Ponge *, D. Raabe

Max-Planck-Institut für Eisenforschung, Max-Planck-Street 1, 40237 Düsseldorf, Germany

Received 30 May 2005; received in revised form 6 July 2005; accepted 6 July 2005
Available online 25 August 2005

Abstract

The mechanical properties of an ultrafine grained 0.2%C–Mn steel, processed by large strain warm deformation and subsequent annealing, have been investigated. The microstructure consists of spheroidized cementite particles in an ultrafine ferrite matrix (average grain diameter ≈1.3 μm). The steel shows an improved combination of strength and toughness when compared with corresponding coarse grained specimens. The reasonable ductility of the steel can be attributed to the finely dispersed cementite particles, which also effectively increase the work hardening rate by the accumulation of geometrically necessary dislocations in their vicinity. The lower shelf energy is significantly higher and the ductile-to-brittle transition temperature is lower in the ultrafine grained steel than in comparable coarse grained specimens. This may be due to the joint effect of grain refinement and delamination in the ultrafine grained steel processed by large strain deformation. The delaminations lead to a decrease in triaxiality of the stress state in the impact test samples. The upper shelf energy is slightly reduced in the ultrafine grained steel, which can be attributed to the effect of delamination.

Keywords: Steel; Warm deformation; Ultrafine grains; Mechanical properties; Ductility

1. Introduction

1.1. Importance of grain refinement for improving mechanical properties of steels

Ultrafine grained steels with relatively simple chemical compositions, strengthened primarily by grain refinement, have great potential for replacing high strength low alloyed steels. The unique feature of grain refinement is that it is the only strengthening mechanism which also increases toughness. Grain refinement of steels which show a ductile-to-brittle transition results in a decrease of the transition temperature [1,2].

For a mild steel processed by flat rolling the average ferrite grain diameter can be reduced from 10 μm (for conventional hot rolling and air cooling) to 5 μm (for controlled rolling and water cooling), thereby, increasing the yield stress by about 80 MPa [3–5]. Based on the Hall–Petch and Cottrell–Petch relationships [6], reducing the grain diameter from 5 to 1 μm would enhance the yield stress by 350 MPa and lower the ductile-to-brittle transition temperature by 200 K. Another decrease of the grain diameter by a factor of five would increase the yield stress further by 680 to over 1000 MPa even for a steel with lean composition [7]. Thus, strong grain refinement to an average grain diameter below 1 μm offers a unique strategy to produce steels with high yield stress and excellent toughness (low ductile-to-brittle transition temperature) at minimal alloying. The main benefits behind such an approach are to avoid additional alloying elements, to skip complicated additional heat treatments like soft annealing, quenching and tempering, and to improve weldability owing to the reduced required content of carbon and other alloying elements when compared to high strength quenched

* Corresponding author.
E-mail address: ponge@mpie.de (D. Ponge).

1359-6454/$30.00
doi:10.1016/j.actamat.2005.07.009

and tempered steels. A further high potential domain for such ultrafine grained steels is the possibility for high strain rate superplasticity at medium and elevated temperatures [8,9].

1.2. Related studies on the mechanical properties of ultrafine grained steels

There are two main groups of methods to produce ultrafine grained steels with a grain diameter of about 1 μm [10–21]. These are the techniques associated with severe plastic deformation [12–17] and advanced thermomechanical processes [18–21]. There are basic differences between these two approaches. Advanced thermomechanical processes are continuous treatments where the phase transformation is essential for the refinement process. The severe plastic deformation techniques are discontinuous methods which are particularly suited to relatively soft materials since quite large strains (i.e., true-strains above 4) are applied in order to obtain ultrafine microstructures.

Several groups [3,22–25] have reported promising tensile properties (at room temperature) of ultrafine grained steels produced either by severe plastic deformation or by advanced thermomechanical processes. Unfortunately, many of the ultrafine grained steels investigated did not display a significant amount of work hardening during tensile testing at room temperature. This shortcoming was in particular reflected by their high yield ratios (lower yield stress/ultimate tensile stress), which, for many ultrafine grained steels, were approximately 1.0, while the yield ratios in conventional steel with similar alloy content are generally close to 0.70. This small amount of work hardening leads typically to the low tensile ductility of ultrafine grained steels with a grain size below 1 μm. According to the work of Park et al. [25], an ultrafine grained low carbon steel (0.15 wt.%C–1.1 wt.%Mn–0.25 wt.%Si) with a grain size of 200 nm, manufactured by severe plastic deformation (accumulative equivalent strain of 4.0 at 623 K), exhibited no work hardening, i.e., necking occurred already in the Lüders regime. Therefore, only a small "uniform" elongation was achieved.

While several reports presented tensile properties of ultrafine grained steels [3,22–25], corresponding Charpy impact properties were rarely investigated due to limitations in the sample size typically available from such laboratory-scale process set-ups.

1.3. Scope of this study

In this study, the mechanical properties of an ultrafine grained 0.2%C–Mn steel produced by large strain warm deformation and annealing were investigated. The data are compared to the mechanical properties of a coarse grained steel with the same composition.

The goal of this study is twofold. First, we aim to obtain a better understanding of the insufficient work hardening rate in ultrafine grained steels, and to use this knowledge to improve the work hardening rate by introducing small spheroidized cementite particles in a fine ferrite matrix. Second, in order to study the Charpy impact properties of the ultrafine grained steel, which were rarely studied in previous investigations, large samples of ~10 mm in thickness were produced by large-scale plane strain compression tests at the Max-Planck-Institut für Eisenforschung. The Charpy impact properties of the ultrafine grained steel, such as the ductile-to-brittle transition temperature, are discussed in detail.

2. Experimental methods

2.1. Specimens and experimental set-up

The chemical composition of the C–Mn steel used in this work was 0.22C–0.21Si–0.74Mn–0.004P–0.003S–0.001N–0.029Al (mass%). The calculated A_{e3} temperature (equilibrium austenite to ferrite transformation temperature) is 1093 K [26]. The laboratory samples were machined directly from the cast ingot into rectangular parallelepiped samples of $50 \times 40 \times 60\ mm^3$ (width × length × height). The plane strain compression tests were conducted by use of a large scale 2.5 MN hot press [27], where the compression direction was parallel to the sample height.

2.2. Outline of the experimental routes for processing the ultrafine grained steel

All specimens were pre-processed by an identical austenitization and cooling route in order to provide a homogeneous ferrite–pearlite microstructure before the application of the different actual thermomechanical techniques [10,28–30]. The basic strategy to obtain a fine transformed ferrite–pearlite microstructure is to use a low austenitization temperature for producing relatively fine austenite. The details of the procedure are as follows: The samples were austenitized at 1193 K (100 K above A_{e3}) for 3 min to achieve a fine austenite grain size. After air cooling to 1143 K, a one-step deformation pass was exerted imposing a logarithmic strain of $\varepsilon = 0.3$ at a strain rate of $10\ s^{-1}$ in order to obtain fully recrystallized austenite. This was followed by a controlled cooling procedure down to the pearlite finish temperature of 823 K at a cooling rate of $6.5\ K\ s^{-1}$ which is the maximum cooling rate to obtain a bainite free ferrite–pearlite microstructure. After this primary treatment which was identical for all specimens, the following different experimental routes were carried out to provide sets of different types of microstructure:

(a) *Conventional route*: In order to study the initial ferrite–pearlite microstructure before large strain warm deformation, a conventional thermomechanical route was applied. This means that after the controlled cooling and 2 min holding period at 823 K as described above the samples were water quenched in order to obtain a bainite-free ferrite–pearlite microstructure.
(b) *Ultrafine grain route*: After a 2 min holding period at 823 K, the large strain warm deformation was performed by applying a four-pass plane strain compression process with an inter-pass time of 0.5 s. Each of the four subsequent steps imposed a logarithmic strain of $\varepsilon = 0.4$ accumulating to a total strain of $\varepsilon = 1.6$. Each pass was conducted at a strain rate of $10\ s^{-1}$. Subsequently, an annealing treatment of 2 h at 823 K was undertaken. The details of the processing can be found in [10].

2.3. Characterization of the microstructure

2.3.1. Light optical microscopy

The specimens for light optical microscopy were mechanically polished to a 1 μm finish and etched using a 1% Nital solution. Micrographs were taken at a sample location where the local strain was equal to the nominal strain according to finite element calculations.

2.3.2. Scanning electron microscopy

We use a JSM-6500F field-emission scanning electron microscopy (SEM). The JSM-6500F offers high lateral resolution and a large probe current density at small probe diameters which is an essential condition for conducting high-resolution electron backscatter diffraction (EBSD) mapping, see following section. Sample preparation for microstructural analysis in the SEM was the same as that for optical metallography.

2.3.3. Microtexture analysis by EBSD

The EBSD measurements were carried out at an accelerating voltage of 15 kV and an emission current of about 100 μA at a specimen inclination angle of 70° towards the camera. Orientation maps were taken at a step size of 100 nm. In the present study, high-angle grain boundaries were defined as homophase interfaces with a misorientation angle of $\theta \geqslant 15°$. Lower values of the local misorientation ($2° \leqslant \theta < 15°$) represent low-angle grain boundaries.

2.3.4. Characterization of grain size

Ultrafine grains produced by large strain deformation in steels are often not completely surrounded by high-angle grain boundaries, but some of the grain boundary segments may have low-angle misorientation character [28]. Compared with low-angle grain boundaries, high-angle grain boundaries are more important for strengthening. Also, high-angle grain boundaries are more efficient in improving the toughness of steels. Therefore, it is necessary to clearly identify and quantitatively characterize the grain boundary character together with the analysis of the grain size [28]. Also, careful characterization of the average grain size is essential for predicting the mechanical properties of steels in terms of the Hall–Petch relationship. For this reason, in this study the ferrite grain size (counting only grains with a grain boundary misorientation $\theta \geqslant 15°$) produced by the ultrafine grain route was measured by use of EBSD maps in conjunction with the mean linear intercept method. The spacing between the grain boundaries was measured both, along the normal direction (ND) and the rolling direction (RD). The grain size is then defined as the average diameter of the equivalent area circles which match the area of the elliptically shaped grains. The ferrite grain size produced by the conventional route was measured by use of the mean linear intercept method.

2.4. Measurement of the mechanical properties

2.4.1. Tensile testing

Quasi-static mechanical characterization was conducted by using tensile test specimens with a round cross section ($\varnothing = 5$ mm) and a gauge length of 25 mm, which were machined in accordance with the corresponding ASTM standard. Tensile tests were conducted at room temperature with a constant crosshead speed of 0.5 mm/min.

2.4.2. Charpy impact test

Subsize Charpy V-notched specimens with a ligament size of $3 \times 4\ mm^2$ were machined along the rolling direction according to the German Industry Norm DIN 50 115. Impact tests were conducted in a temperature range from 103 to 423 K. Temperature measurement was carried out during impact testing by using a thermocouple soldered to the specimen. The value of the ductile-to-brittle transition temperature (DBTT) was determined from the Charpy curve as the temperature corresponding to the half value of the upper shelf energy. The results obtained on such subsize specimens were converted to values valid for full size specimens (EN 10 045) by using the correlations recommended in [31].

3. Experimental results

3.1. Microstructures obtained from the conventional and ultrafine grain routes

The microstructure of the steel after the conventional route (without large strain warm deformation) consists of ferrite and pearlite (Fig. 1(a)). After the large strain

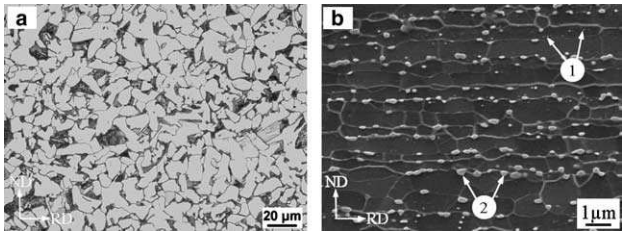

Fig. 1. (a) Light optical micrograph of the initial ferrite–pearlite microstructure of the steel processed by the conventional route (without large strain warm deformation). (b) SEM image of the ultrafine grained steel processed by the ultrafine grain route (with warm deformation, $\varepsilon = 0.4 \times 4$, and subsequent 2 h annealing at 823 K). The white markers (number 1) highlight the dispersion of cementite particles inside the ferrite grains and the alignment of cementite particles along the ferrite grain boundaries (number 2).

warm deformation ($\varepsilon = 1.6$) and subsequent annealing at 823 K for 2 h (ultrafine grain route), the microstructure consists of ferrite with a small grain size and globular cementite particles (Fig. 1(b)). Smaller cementite particles (5–90 nm) are distributed inside the ferrite grains (see arrows 1). Planar arrays of larger cementite particles (90–350 nm) are located at the ferrite grain boundaries (see arrows 2), acting as obstacles to the migration of ferrite grain boundaries in the normal direction. The average ferrite grain sizes in the initial ferrite–pearlite microstructure (Fig. 1(a)) and in the ultrafine microstructure (Fig. 1(b)) are 6.8 and 1.3 μm, respectively. Further details of the microstructure were reported earlier in [10].

3.2. Comparison of the mechanical properties between the conventional and ultrafine grained steels

3.2.1. Tensile properties

Fig. 2 shows the tensile properties of the conventional and the ultrafine grained steels at room temperature. The decrease in grain size from 6.8 to 1.3 μm leads to an increase in strength (especially of the lower yield stress) and in Lüders strain. The ductility of the ultrafine grained steel decreases. The total elongation yields about 20%.

Fig. 3 shows details of the tensile properties. Each symbol represents an average value obtained from three separate tensile tests. The decrease in the average ferrite grain size from 6.8 to 1.3 μm leads to an increase of the lower yield stress by 49% (Fig. 3(a)), of the ultimate tensile stress by 14% (Fig. 3(a)), of the yield ratio by 30% (Fig. 3(b)), and of the Lüders strain by 39% (Fig. 3(c)). The decrease in grain size also results in a drop of the uniform and of the total elongation by 43% and 33%, respectively (Fig. 3(d)).

3.2.2. Charpy impact properties

Fig. 4 shows the impact transition curves of the steels for subsize specimens. Compared with the conventional steel the upper shelf energy is decreased

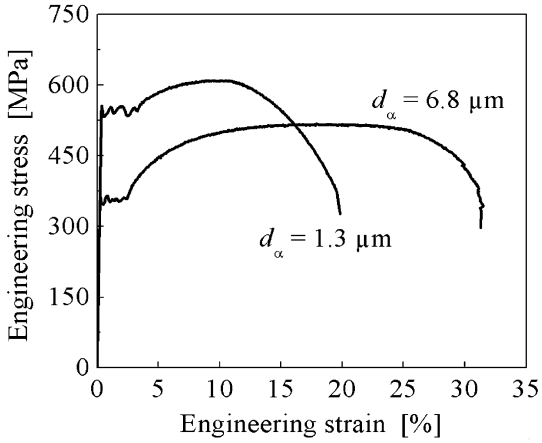

Fig. 2. Comparison of engineering stress–strain curves of the steels with different ferrite grain sizes. The different grain sizes were produced by the conventional route (without large strain warm deformation) and the ultrafine grain route, respectively. The ultrafine grain route involved a warm deformation procedure with four steps (each deformation step with $\varepsilon = 0.4$ and $\dot{\varepsilon} = 10\ s^{-1}$) and a subsequent 2 h annealing treatment at 823 K. The symbol d_α refers to the average ferrite grain diameter.

and the sigmoidal curve is flatter in the ultrafine grained steel. As introduced above, the DBTT is defined as the temperature at half of the upper shelf energy. Fig. 4 shows that the decrease in grain size leads to a decrease in the ductile-to-brittle transition temperature. In the ductile-to-brittle transition region the absorbed energy changes slightly with temperature for the ultrafine grained steel.

It is important to note that the lower shelf energy of the ultrafine grained steel is much higher than that of the conventional steel. For example, in Fig. 4, the absorbed energy amounts to about 2 J for the ultrafine grained steel at an impact test temperature of 103 K. In contrast, it yields only about 0.5 J for the conventional steel tested even at 143 K. Figs. 5(A) and (B) show the fracture surfaces of the ultrafine grained steel and of the conventional steel tested at 103 K and 143 K, respectively. In Fig. 5(a), the fracture surface of the ultrafine grained steel consists of both smooth delaminations/splits and dimpled fracture, in alternating sequence. Nearly 50% shear fracture can be observed in the fracture surface. If the DBTT is defined by the temperature at which 50% of the fracture surface is shear fracture, the DBTT of the ultrafine grained steel is approximately 103 K for the subsize specimen. The details of the contributions of smooth delamination and dimpled fracture are shown in Fig. 5(b)–(d). The observation area is in the middle of the thickness (along ND), about 1 mm away from the V-notch. The reason to select this location as the area of observation is because the stress state during impact testing at this position promotes a more brittle fracture. In contrast to the ultrafine grained specimen, in the conventional steel a complete cleavage fracture (nearly 100%) occurs already at 143 K, Fig. 5(e) and (f).

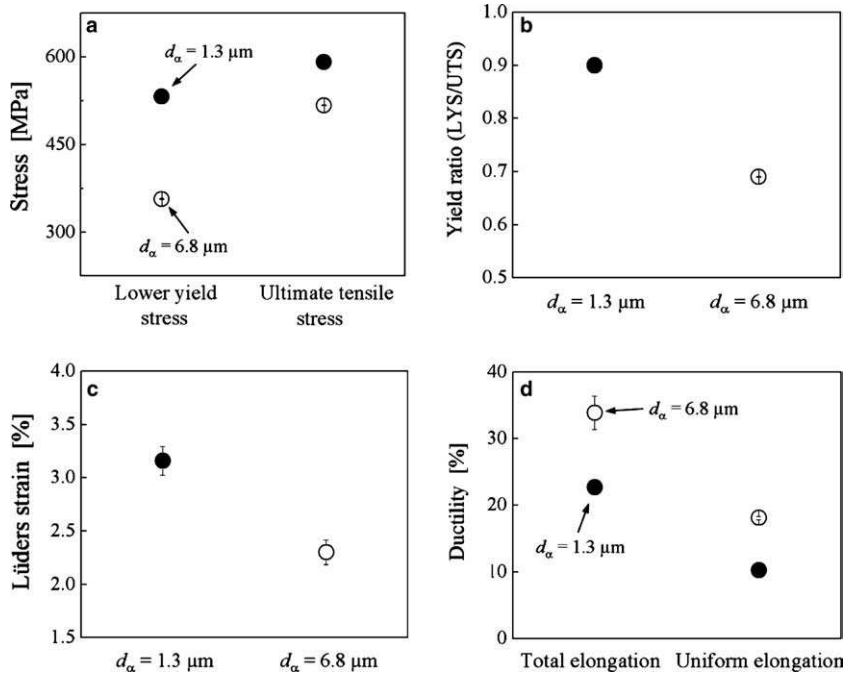

Fig. 3. Comparison of the tensile properties at room temperature of the steels with different ferrite grain sizes. The symbol d_α refers to the average ferrite grain diameter. (a) strength; (b) yield ratio: lower yield stress/ultimate tensile stress (LYS/UTS); (c) Lüders strain; (d) ductility.

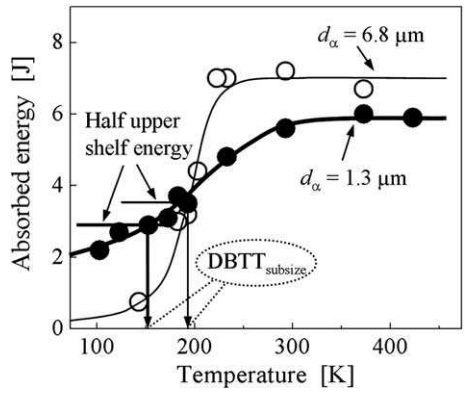

Fig. 4. Dependence of the Charpy impact properties on temperature of the steels with different ferrite grain sizes. The symbol d_α refers to average ferrite grain diameter. DBTT$_{subsize}$: ductile-to-brittle transition temperature of subsize specimen with a ligament size of 3×4 mm^2. The ductile-to-brittle transition temperature was determined by using the correlations recommended in [31].

Fig. 6(a) shows the SEM image of the same ultrafine grained steel after the Charpy impact test at 103 K (Fig. 5(a)) but measured this time in the transverse direction of the specimen. The serrated area of the sample close to the fracture surface (Fig. 6(a)) displays the alternating ductile and delaminated areas of the fracture surface (Fig. 5(a)). The white arrows in Fig. 6(a) point out chains of large voids in the specimen in front of the actual fracture surface, which are aligned parallel to RD. Figs. 6(b) and (c) show large magnification of the crack along RD and the area below a shear surface, respectively, in terms of microtexture maps taken by EBSD. The orientation maps show the crystalline directions parallel to ND as indicated by the colors in the stereographic triangle, Fig. 6(c). Fig. 6(b) shows mainly two colors at the tip of the crack, namely, red and blue indicating the texture components of ⟨1 1 1⟩‖ND (in blue) and ⟨0 0 1⟩‖ND (in red). It can be seen that the crack separates the elongated clusters of grains with different texture components of ⟨1 1 1⟩‖ND and ⟨0 0 1⟩‖ND, which demonstrates that the crack spreads along the boundaries of grains (e.g., grain "1" and "2") with different orientations (i.e., high-angle grain boundary misorientation). Fig. 6(c) shows the ND orientation map below a shear fracture. Compared to Fig. 6(b), the ⟨1 0 1⟩‖ND texture component is the majority in Fig. 6(c). This is due to the bending during the Charpy impact test. An aligned damage (highlighted by the ellipse) below the shear fracture can be seen clearly.

The values of the Charpy impact properties for the ultrafine grained and the conventional steels, calculated for full size specimens according to [31], are summarized in Fig. 7. The data reveal that grain refinement leads to a decrease in both the "specific" upper shelf energy (related to the ligament area) and the DBTT.

In order to understand why the ultrafine grained steel shows a reduced upper shelf energy compared with the coarse grained specimens, the fracture surfaces of the steels in the upper shelf region were investigated in detail. Fig. 8(a) and (b) shows the fracture surfaces of both steels after Charpy impact testing at room temperature.

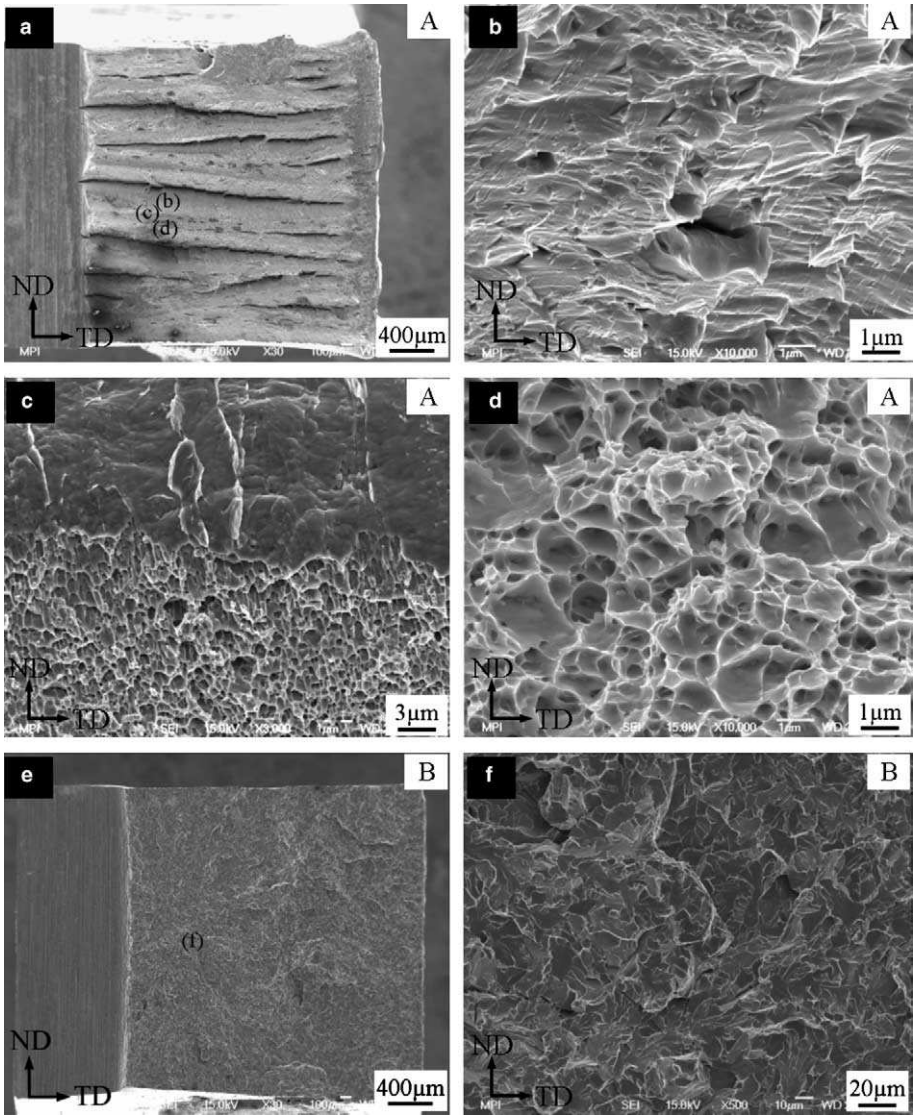

Fig. 5. SEM micrographs of the fracture surfaces of the steels with different ferrite grain sizes after the Charpy V-notch impact tests: (A) Fracture surface of the ultrafine grained steel after impact testing at 103 K. (a) total view of the fracture surface; (b) smooth delamination surface; (c) border area between delamination surface and shear fracture; (d) shear fracture. Observation areas of (b)–(d) are shown in (a). (B) Fracture surface of the conventional steel after impact testing at 143 K. (e) total view of the fracture surface; (f) appearance of the cleavage fracture, observation area is shown in (e).

Compared to a complete shear fracture surface in the conventional steel (Fig. 8(a)), a few delaminations (indicated by black arrows in Fig. 8(b)) can be observed in the ultrafine grained steel (Fig. 8(b)). The delamination in the ultrafine grained steel becomes more pronounced with decreasing testing temperature. For example, Fig. 8(c) shows a continuous delamination which extends almost through the entire fracture surface in the ultrafine grained specimen at a test temperature of 233 K. With a further decrease in the test temperature to 103 K, the length and number of these continuous delaminations increase, Fig. 8(d). The effect of grain refinement on lower yield stress and transition temperature is summarized in Fig. 9. The decrease in grain size from 6.8 μm to 1.3 μm leads to an increase in yield stress and a decrease in ductile-to-brittle transition temperature, i.e., to an improved combination of strength and toughness.

4. Discussion

4.1. Tensile properties

4.1.1. Strength

Compared with the tensile properties of the conventional steel, a substantial enhancement of the strength is found for the ultrafine grained steel, Fig. 3(a). Numerous investigations have shown that the yield stress of low-carbon steel increases in inverse proportion to the

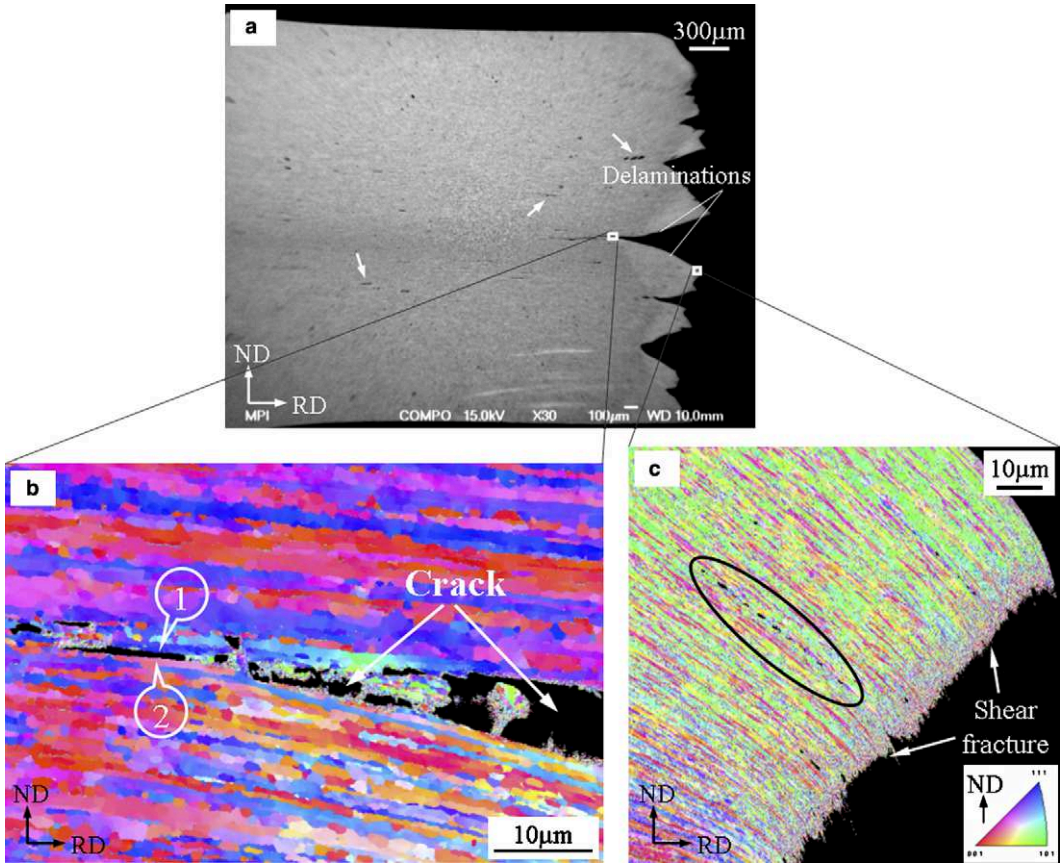

Fig. 6. SEM image and ND orientation maps (taken by the EBSD measurement) of the ultrafine grained steel after Charpy impact testing at 103 K; the specimen shown in Fig. 5(a) but measured this time in the transverse direction (TD) of the sample. Orientation components in (b) and (c), ⟨1 1 1⟩‖ND in blue, ⟨0 0 1⟩‖ND in red and ⟨1 0 1⟩‖ND in green. (a) Total view of the sample in TD. The white arrows point out chains of large voids in the specimen. (b) Front of a crack. The circles 1 and 2 show two elongated grains with high–angle grain boundaries in between. (c) Aligned damage below a shear fracture. The ellipse highlights the alignment of voids along the grain boundaries.

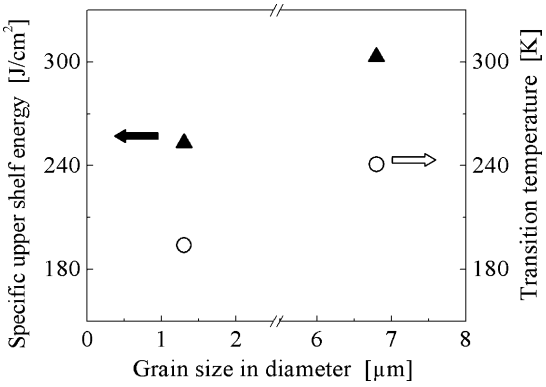

Fig. 7. Charpy impact properties of the steels with different ferrite grain sizes. The symbol d_α refers to average ferrite grain diameter. The specific upper shelf energy and the transition temperature in this context are the energy and temperature related to the ligament area for a full size specimen. These were converted from the results of subsize specimens by using the correlations recommended in [31].

square root of the ferrite grain size in terms of the Hall–Petch relationship.

It is important to note in this context that the ultrafine grained steel contains dislocations and corresponding substructures inside the ultrafine grains [10] as well as an elongated grain morphology in the microstructure, Fig. 1(b). This means that the increase in strength for the ultrafine grained specimens is caused not only by grain refinement strengthening but also by residual work hardening and crystallographic texture strengthening. Nevertheless, the latter two strengthening mechanisms do not change the tensile properties to the same degree as the reduced grain size. Thus, it is plausible that grain refinement is the main factor in improving the strength of the ultrafine grained steel investigated.

4.1.2. Ductility

One of the unusual aspects of ultrafine grained steels is their relatively low tensile ductility at room temperature (especially the uniform elongation) compared with their coarse grained counterparts. This applies also in the current case. The data shown in Fig. 2 indicate that the amount of work hardening is reduced by grain refinement. This is reflected by a higher yield ratio (lower yield stress/ultimate tensile stress) of about 0.90 for the ultrafine grained steel compared with a ratio of 0.7 for the conventional steel, Fig. 3(b). The reason for

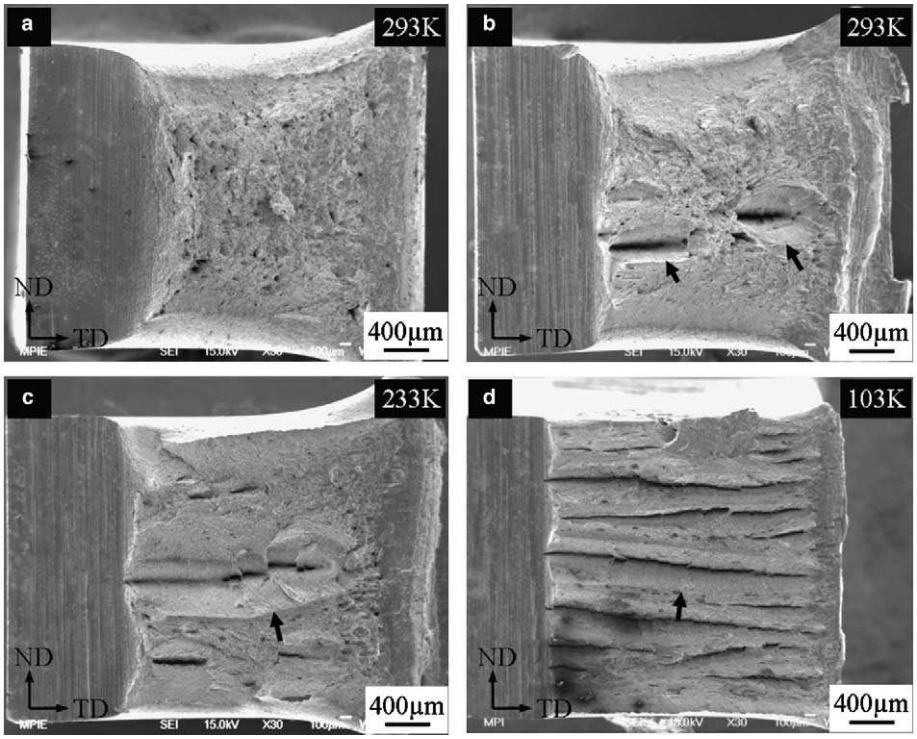

Fig. 8. Fracture surfaces of the steels with different ferrite grain sizes after Charpy V-notch impact tests (SEM): (a) Fracture surface of the conventional steel after impact testing at 293 K; (b), (c) and (d) fracture surfaces of the ultrafine grained steel after impact testing at 293, 233 and 103 K, respectively. The black arrows point out material delaminations.

the decrease in tensile ductility at room temperature for the ultrafine grained steel can be explained as follows:

First, dynamic recovery as a softening mechanism is able to reduce the apparent work hardening rate. During tensile deformation, the dislocations that carry the intragranular strain are trapped at grain boundaries. Especially in ultrafine grained steels, the kinetics of dynamic recovery is associated with the spreading of trapped lattice dislocations into grain boundaries [32–34]. The change of the dislocation density during dynamic recovery in terms of the trapped lattice dislocations spreading into the grain boundaries was studied in detail by Park et al. [25]. The authors calculated the approximate times for dislocations spreading into grain boundaries. These showed that for ultrafine grained steels, the time for dislocations spreading into grain boundaries is shorter than the deformation time of the tensile test. This decrease in dislocation density leads to no significant accumulation of dislocations inside the grains and, consequently, to less work hardening when compared with corresponding steels of large grain size. Following these earlier investigations, we assume that there are two kinds of recovery mechanisms, namely, slow recovery in the grain interiors and much faster recovery in the vicinity of grain boundaries. In coarse grained steels, the latter was not clearly observed due to a lower volume fraction of the overall volume near grain boundaries. Using data from the present study, where the grain diameter was reduced from 6.8 to 1.3 μm, this grain refinement can be expected to enhance the volume fraction of the overall volume near grain boundaries by a factor of about five. Thus, in ultrafine grained steels, such faster recovery near grain boundaries seems to be significant.

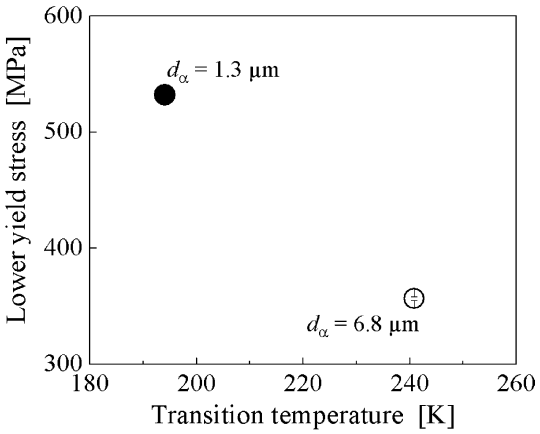

Fig. 9. Lower yield stress and ductile-to-brittle transition temperature of the steels. The results from the coarse grained and ultrafine grained steels are displayed by open and filled symbols, respectively. The symbol d_α refers to average ferrite grain diameter.

Second, the decrease in tensile ductility can be explained in terms of plastic instabilities, which initiate necking due to excessive localized deformation. The condition for the initiation of necking in a tensile test is indicated by the Considère criterion [35], $\sigma_t = d\sigma_t/d\varepsilon_t$. When

the slope of the true-stress true-strain curve (work hardening rate), $d\sigma_t/d\varepsilon_t$, is equal to the true-stress, σ_t, uniform deformation stops and necking is initiated. As mentioned above, ultra grain refinement greatly increases the flow stress of steels, especially during the early stages of plastic deformation. On the other hand, the present work also revealed that grain refinement led to a reduced work hardening capacity. As a result, plastic instability (necking) occurs at an early stage during tensile testing, which results in a limited uniform elongation in ultrafine grained steels.

The yield ratio is high in ultrafine grained steels, Fig. 3(b). However, despite the high strength, good ductility can still be obtained, as documented by the total elongation of about 20% and the uniform elongation of about 10%, Fig. 3(d). These values differ from the results reported in previous studies which presented total elongations of not more than 10%. The good ductility in the present case can be attributed to the presence of finely dispersed cementite particles, which improve the work hardening capacity [29]. A large volume fraction and a fine dispersion of the cementite particles effectively increases the work hardening rate by promoting the accumulation of geometrically necessary dislocations around the particles [36,37].

4.1.3. Lüders strain

In Fig. 3(c), the decrease in grain size led to an increase in the Lüders strain. A large Lüders strain has been noted previously by Lloyd and Morris [38] in a fine grained (1–3 μm) Al–6%Ni alloy that contained small amounts of magnesium in solid solution. They observed that the reduction of grain size entailed a drop in yield stress and a decrease in work hardening. Hayes and Wang [39,40] conducted a study on the influence of grain refinement on the Lüders strain in Al alloys. They investigated the serrated strain regime for specimens with various grain sizes between 0.4 and 20 μm and observed that the Lüders strain was linearly proportional to the inverse square root of the grain size in Al alloys, as in the Hall–Petch relationship. The appearance of pronounced yield drops and very large Lüders strain regimes thus appear to be characteristics of ultrafine grained Al alloys [39]. These phenomena can be linked to an instantaneous low density of mobile dislocations, the lack of dislocation sources within grains, and the low work hardening rate of ultrafine grained alloys.

The serrated flow that characterizes the propagation of plastic strain within a Lüders band is governed by the dynamic interplay of micromechanical hardening and softening. The Lüders regime with its dynamic balance is, therefore, determined by the locking state of the dislocations, the hardening coefficient, the softening coefficient, the strain rate and the temperature [29]. In the present study, yielding of the steels investigated took place in the form of deformation bands initiated due to local stress concentrations. Owing to the high density of mobile dislocations formed by unlocking and by dislocation multiplication, the material within this deformation band effectively softens and undergoes localized plastic deformation. As mentioned in Section 4.1.2, dynamic recovery is pronounced in steels with smaller grain sizes owing to fast recovery in the vicinity of grain boundaries [25]. A decrease in the work hardening rate in the ultrafine grained steel, which can be attributed to the rapid dynamic recovery, leads to stress saturation at large strains. This amounts to slow propagation of the Lüders band front for the steel with the fine microstructure.

4.2. Toughness

4.2.1. Effect of grain refinement

A reduction in the average grain size commonly leads to a lower DBTT (Fig. 4). This can be understood in terms of cleavage crack initiation and propagation. It is known that the grain size is one of the major factors determining the cleavage fracture unit [41,42]. According to the work of Kim and Brozzo [41,42], the cleavage fracture unit is the length of a cleavage crack between two neighboring breakthrough points in its propagation direction, which is reduced as the grain size decreases. When the cleavage crack propagates through several grains, both the emission of crack-tip dislocations and the formation of cleavage facets are interrupted by the grain boundaries. If the cleavage crack moves across a high-angle grain boundary, the crack front must be branched, which, together with the separation of the grain boundary between the breakthrough points, result in an additional portion of fracture work. This toughening effect can lower the DBTT considerably [43,44]. For example, when the cleavage crack paths are carefully observed at high magnifications, it can be seen that the paths are changed by high-angle grain boundaries. Furthermore, it was observed that cleavage cracks can also be impeded by high-angle grain boundaries [45]. Thus, a decrease in grain size can limit the propagation of initiated cleavage cracks and raise the fracture toughness in the transition region.

The ductile-to-brittle transition of a body-centered cubic material is accompanied by a change in the fracture mechanism from void coalescence to cleavage. Thus the DBTT can be quantitatively interpreted as a result of the competition between the flow stress and the cleavage fracture stress of the material [46]. According to the Hall–Petch relation [6], grain refinement contributes to an increase in the yield stress. On the other hand, grain refinement effectively enhances the cleavage fracture stress. Since the DBTT is the point at which the yield stress is equal to the cleavage fracture stress, therefore, the DBTT is lowered by grain refinement due to a more

significant increase in the cleavage fracture stress than in the yield stress.

Grain refinement leads to an improvement in toughness. Nevertheless, the morphology of pearlite or cementite has complex effects on the impact properties. Coarse rod-type and spherical-type cementite particles are considered as initiation sites for damage [47] and are major detrimental microstructural features in steels [46]. This is due to the low adhesion between the second phase and the matrix and to differences in their elastic and plastic properties [48]. It was assumed that, compared with lamellar cementite, spherical cementite particles exert a less drastic effect on toughness. However, for the occurrence of cleavage fracture, the free distance of two neighboring high-angle grain boundaries (Griffith type crack length) seems to be more important than the shape and dispersion of the particles. The pronounced effect of grain refinement on improving toughness has been reported in [30].

4.2.2. Shelf energy

The ductile-to-brittle transition in steels is associated with two different failure mechanisms. At high temperatures in the upper shelf region, fracture occurs by the nucleation and coalescence of microvoids entailing ductile tearing. This process requires extensive plastic deformation and, therefore, large amounts of energy. At low temperatures, fracture occurs by cleavage, which is the sudden separation of atomic planes across the specimen [49,50]. In this case, less energy is required.

4.2.2.1. Lower shelf energy. Fig. 4 shows that the lower shelf energy is significantly higher in the ultrafine grained steel than in the coarse grained steel. On the one hand, this can be attributed to the effect of grain refinement on improving toughness even at very low temperatures, which is documented by the presence of about 50% shear fracture in the ultrafine grained subsize specimen when the test temperature was as low as 103 K. On the other hand, this phenomenon can be related to the anisotropic microstructure or pronounced crystallographic texture of the ultrafine grained steel produced by the large strain deformation below the A_1 temperature (austenite to pearlite transformation finish temperature).

After the large strain deformation, a strong alignment of the microstructure was formed along the rolling direction, Fig. 6(a). In Fig. 6(a), the chains of voids along the RD were visible. A large magnification of the crack tip, Fig. 6(b), showed that the path of crack propagation was located between two elongated grains which were separated by a high-angle grain boundary (i.e., grain "1" and grain "2"). This observation demonstrates that a high-angle grain boundary acts as a favorable path for crack propagation. This is preferred when large cementite particles are located at the ferrite grain boundaries, e.g., see the alignment of voids along the grain boundaries in Fig. 6(c). The alternating microstructure of ferrite and aligned cementite particles facilitates the spread of cracks (below the V-notch) not only in the transverse direction but also in the rolling direction, Figs. 5(a) and 6(a) and (b).

Figs. 6(a) and (b) showed that the delaminations follow along the elongated grain boundaries. The occurrence of the delamination along the grain boundaries both above and below an elongated grain indicates that the delamination can make minor adjustments in its propagation direction to switch from one grain boundary to another. The high-magnification view of the fracture surface for the ultrafine grained steel tested at 103 K clearly showed the smooth delamination surface as well as the dimpled ductile fracture area (Fig. 5(c)). Close examination of the delamination revealed a relatively smooth undulating surface, Fig. 5(b), which suggests some type of decohesion of the grain boundaries. This is also confirmed by the observation that two elongated grains (i.e., grain "1" and grain "2" in Fig. 6(b)) with different texture components, $\langle 1\,1\,1\rangle \| \mathrm{ND}$ and $\langle 0\,0\,1\rangle \| \mathrm{ND}$, respectively, were separated by a crack. The delaminations appear to propagate by means of a low-energy fracture mechanism that produces a fairly smooth fracture surface. This fracture does not exhibit the typical cleavage appearance with a strong (1 0 0) texture [51].

The emergence of the delaminations has not so far been sufficiently explained. From previous studies it seems that features like bent ferrite–pearlite microstructures [50], elongated ferrite grain shapes [51], certain texture characteristics [52], and aligned particles and inclusions [53] favor the occurrence of delamination. According to [54], the phenomenon of delamination does not have a direct influence on the speed of crack growth in ductile failure. Nevertheless, delamination leads to a reduction of the DBTT, which can be explained as follows.

The stress state at the crack tip determines the extent of fracture toughness, which increases with decreasing tensile triaxiality. Tensile triaxiality can be reduced by relaxing the σ_{zz} stress component (Fig. 10) by the delamination of interfaces that are perpendicular to the normal direction (thickness direction). When delamination occurs, the effective thickness of the sample is reduced and the σ_{zz} stress decreases to zero at each delamination. Eventually, the specimen acts like a cluster of thin samples instead of one thick sample, Fig. 5(a). For this reason, the extent of the shift in the DBTT depends on the number of weak planes introduced into the specimen, i.e., the more subsections are introduced, the thinner the delaminated segments will be and the larger the tendency for plane stress. In the present study, each interface of ferrite and aligned cementite particles acts like a weak plane. The more aligned cementite particles are present, the more weak planes are introduced and the

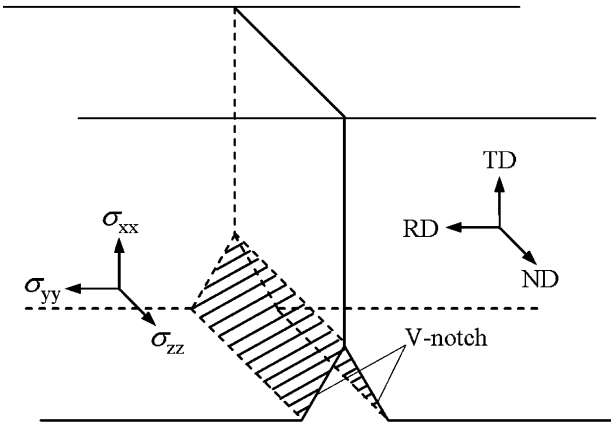

Fig. 10. Geometry of a notch and directions of the stresses. σ_{xx}, σ_{yy} and σ_{zz}: normal stresses in the x-, y- and z-directions, respectively. The direction of σ_{zz} is parallel to the notch front. The biaxial stress state at the free surface is plane stress ($\sigma_{zz} = 0$).

higher the possibility of delamination. As a result, a higher fracture toughness or a lower ductile-to-transition temperature can be expected.

On the other hand, the distribution of sulphides, which exist as manganese sulphides in most structural steels, is different in the rolling, transverse and thickness directions [49]. After large strain deformation, a high notch impact energy is expected in the rolling direction due to the low density of hetero-interfaces between the matrix and inclusions along the crack path (below the V-notch and along the TD). Due to the very low sulphur content (0.003 mass%) in the steel investigated, there should be no significant effect of manganese sulphide on the anisotropy.

4.2.2.2. Upper shelf energy. Fig. 7 shows a lower specific upper shelf energy in the ultrafine grained steel if compared with the conventional steel. On the one hand, this may be due to the relatively low ductility of this steel, which is documented by the smaller integrated area below the engineering stress–strain curve before necking, Fig. 2. Another reason can be attributed to the appearance of some delaminations in the ultrafine grained steel tested even in the upper shelf region.

Compared to a complete shear fracture surface in the conventional steel (Fig. 8(a)), a few delaminations can be observed in the ultrafine grained steel (Fig. 8(b)) when the Charpy impact test was carried out at room temperature (in the upper shelf region). Since there is only minor plastic deformation in the area of the delamination, less consumption of energy and a reduced fracture toughness can be expected in the ultrafine grained steel (Fig. 8(b)) compared with the conventional steel with a complete shear fracture (Fig. 8(a)). This is different from the case in the lower shelf energy region, where the decrease in the DBTT is evident due to the change in the stress triaxiality associated with relaxing σ_{zz}. As a result, a lower upper shelf energy and a lower DBTT were obtained in the ultrafine grained steel processed by large strain warm deformation (Fig. 7).

According to the work of Fujioka et al. [55], a reduction of the upper shelf energy was also observed in a 0.16C–0.44Si–1.33Mn–0.012Ti–0.013Nb steel with a grain size of 1.5 μm. The ultrafine grained steel in their study was produced by flat rolling with a total logarithmic strain of $\varepsilon \approx 2.5$ at 973 K. They attributed the reduced value of the upper shelf energy to the elongated grain morphology in the ultrafine grained steel. However, in the study of Nagai [21] the same value of upper shelf energy was found for an ultrafine and a coarse grained steel (0.15C–0.3Si–1.5Mn) with grain sizes of 0.9 and 20 μm, respectively. The ultrafine grained steel was fabricated by warm rolling using caliber rolls. The sample was rotated 90° about the rolling direction after each pass in order to conduct multi-directional deformation. The upper shelf energy was unexpectedly high, which was explained by the high cleanness of the steel investigated [21].

According to our investigation and earlier reports in the literature on the shelf energy of ultrafine grained steels [21,55], the reduced value of the upper shelf energy in two-phase ultrafine grained materials may be mainly due to the anisotropic microstructure resulting from the large strain deformation. Unfortunately, large strain deformation at a low deformation temperature is currently a favorable method to produce ultrafine grained microstructures. Therefore, it might be particularly attractive in the future to develop ultrafine grained steels by the use of relatively low strains and high temperatures.

5. Conclusions

An excellent combination of strength and toughness was obtained in an ultrafine grained 0.2%C–Mn steel produced by large strain warm deformation. Significant work hardening led to reasonable ductility in the ultrafine grained steel, which is documented by about 10% uniform elongation and 20% total elongation. Grain refinement also resulted in an increased Lüders strain. Our main conclusions are:

(1) The reasonable ductility obtained can be attributed to the presence of finely dispersed cementite particles, which improved the work hardening capacity owing to the accumulation of geometrically necessary dislocations around the particles.
(2) The ultrafine grained steel was characterized by a large Lüders strain. This effect can be explained by the low density of mobile dislocations and the relatively low work hardening rate due to the rapid dynamic recovery of ultrafine grained steel compared to coarse grained steel.

(3) In the ultrafine grained steel, the upper shelf energy was relatively low, this can be attributed to the occurrence of delaminations. The alignment of cementite particles along the ferrite grain boundaries in the rolling direction and the crystallographic texture promoted the formation of delaminations.
(4) The lower shelf energy was significantly raised and the DBTT was lower in the ultrafine grained steel compared to the coarse grained steel. This can be attributed to the joint effect of the small ferrite grain size and the occurrence of delamination, which entailed a decrease in the triaxiality of the stress state in the impact test samples of the ultrafine grained steel.

Acknowledgements

The authors express their gratitude for the financial support of the European Coal and Steel Community (ECSC). Project title: ultrafine grained steel by innovative deformation cycles; number: 7210-PR/288.

References

[1] Pickering FB. Physical metallurgy and the design of steels. London: Applied Science Publishers; 1978. p. 16.
[2] Gladman T, Pickering FB. The effect of grain size on the mechanical properties of ferrous materials. In: Baker TN, editor. Yield, flow and fracture of polycrystals. London: Applied Science Publishers; 1983. p. 148.
[3] Hodgson PD, Hickson MR, Gibbs RK. Scripta Mater 1999;40:1179.
[4] Priestner R, Ibraheem AK. Mater Sci Technol 2000;16:1267.
[5] Hickson MR, Hurley PJ, Gibbs RK, Kelly GL, Hodgson PD. Metall Mater Trans A 2002;33:1019.
[6] Kozasu I. Processing – thermomechanical controlled processing. In: Cahn RW, Haasen P, Kramer EJ, editors. Material science technology, vol. 7.. Weinheim: VCH; 1992. p. 190.
[7] Ibraheem AK, Priestner R, Bowen JR, Prangnell PB, Humphreys FJ. Thermomechanical processing of steels. London: The Chameleon Press; 2000. p. 446.
[8] Mayo MJ. Nano Mater 1997;9:717.
[9] Shah S, Chokshi AH. Colloids Surf A Physicochem Eng Aspects 1998;133:57.
[10] Song R, Ponge D, Raabe D, Kaspar R. Acta Mater 2005;53:845.
[11] Han BQ, Yue S. Mater Proc Technol 2003;136:100.
[12] Valiev RZ. Mater Sci Eng A 1997;234:59.
[13] Segal VM. Mater Sci Eng A 1999;271:322.
[14] Saito Y, Utsunomiya H, Tsuji N, Sakai T. Acta Mater 1999;47:579.
[15] Tsuji N, Ueji R, Minamino Y. Scripta Mater 2002;47:69.
[16] Inoue T, Torizuka S, Nagai K. ISUGS 2001. Fukuoka, Japan: The Iron and Steel Institute of Japan; 2001. p. 88.
[17] Horita Z, Fujinami T, Langdon TG. Mater Sci Eng A 2001;318:34.
[18] Kaspar R, Distl JS, Pawelski O. Steel Res 1988;59:421.
[19] Matsumura Y, Yada H. ISIJ Int 1987;27:492.
[20] Najafi-Zadeh A, Jonas JJ, Yue S. Metall Trans A 1992;23:2607.
[21] Nagai K. Mater Proc Technol 2001;117:329.
[22] Song R, Kaspar R, Ponge D, Raabe D. Ultrafine grained materials III. Charlotte, NC: TMS; 2004. p. 445.
[23] Liu M, Shi B, Bi G, Cao H, Cai X, Song H. Mater Sci Eng A 2003;360:101.
[24] Hickson MR, Hodgson PD. Mater Sci Technol 1999;15:85.
[25] Park KT, Kim YS, Lee JG, Shin DH. Mater Sci Eng 2000;293:165.
[26] Jansson B, Schalin M, Sundman B. J Phase Equil 1993;14:557.
[27] Kaspar R, Pawelski O. Materialprüfung 1989;31:14.
[28] Song R, Ponge D, Kaspar R, Raabe D. Z Metallkd 2004;95:513.
[29] Song R, Ponge D, Raabe D. Scripta Mater 2005;52:1075.
[30] Song R, Ponge D, Kaspar R. Steel Res 2004;75:33.
[31] Kaspar R, Faul H. MP Materialprüfung 2001;43:18.
[32] Valiev RZ, Kozlov EV, Ivanov YF, Lian J, Nazarov AA, Baudelet B. Acta Metall Mater 1994;42:2467.
[33] Lian J, Baudelet B, Nazarov AA. Mater Sci Eng A 1993;172:23.
[34] Lojkowski W. Acta Metall Mater 1991;39:1891.
[35] Reed-Hill RE, Abbaschian R. Physical metall principles. Boston (MA): PWS Publishing; 1994. p. 158.
[36] Ashby MF. Philos Mag 1970;21:399.
[37] Fisher JC, Hart EW, Pry RH. Acta Mater 1953;1:336.
[38] Lloyd DJ, Morris LR. Acta Metall 1977;25:857.
[39] Hayes JS, Keyte R, Prangnell PB. Mater Sci Technol 2000;16:1259.
[40] Wang ZC, Prangnell PB. Mater Sci Eng A 2002;328:87.
[41] Kim S, Im YR, Lee S, Lee HC, Oh YJ, Hong JH. Metall Mater Trans A 2001;32:903.
[42] Brozzo P, Buzzichelli G, Mascanzoni A, Mirabile M. Metal Sci 1977;11:123.
[43] Hulla D. Acta Metall 1960;8:11.
[44] Ritchie RO, Knott JF, Rice JR. J Mech Phys Solids 1973;21:395.
[45] Kim S, Lee S, Lee BS. Mater Sci Eng A 2003;359:198.
[46] Im YR, Oh YJ, Lee BJ, Hong JH, Lee HC. J Nucl Mater 2001;297:138.
[47] Broek D. Eng Fract Mech 1973;5:55.
[48] Petch NJ. Iron Steel Inst 1953;174:25.
[49] Pitsch W, Sauthoff G, Hougardy HP. Steel. In: Verein Deutscher Eisenhüttenleute, editor. A handbook for mater research and engineering, vol. 1. Berlin: Springer-Verlag; 1992. p. 278.
[50] Shanmugam P, Pathak SD. Eng Fract Mech 1996;53:991.
[51] Bramfitt BL, Marder AR. Metall Trans A 1977;8:1263.
[52] Schofield R, Roentree G, Sarma NV, Weiner RT. Metals Technol 1974:325.
[53] McEvely AJ, Rush RH. Trans ASM 1962;55:654.
[54] Miyoshi E, Fukuda M, Iwanaga H, Okazawa T. In: Proceedings of Institute of Gas Engineering Conference, crack propagation in pipe lines; 1974. paper 4.
[55] Fujioka M, Yokota T, Adachi Y, Matsukura N. In: Proceedings of the second symposium on super metal. Japan; 1999. p. 193.